Finite-size effects and short-range crystalline order in Si and SiO_2 studied by X-ray absorption fine structure spectroscopy

1993 J. Phys.: Condens. Matter 5 5377

(http://iopscience.iop.org/0953-8984/5/31/003)

J. Phys.: Condens. Matter 5 (1993) 5377–5388. Printed in the UK

Finite-size effects and short-range crystalline order in Si and SiO_2 studied by x-ray absorption fine structure spectroscopy

G R Harp†¶, D K Saldin†‡ and B P Tonner†§

† Department of Physics, University of Wisconsin–Milwaukee, Milwaukee, USA
‡ Laboratory for Surface Studies, University of Wisconsin–Milwaukee, Milwaukee, USA
§ Synchrotron Radiation Center, University of Wisconsin-Madison, Madison, USA

Received 22 February 1993, in final form 26 May 1993

Abstract. The x-ray absorption near-edge structures from the Si 2p edge have been measured at high resolution, and compared to a theoretical calculation using a cluster multiple-scattering model. The absorption features near threshold are shown to be sensitive to the degree of short-range crystalline order, over a range of up to 40 Å. The real-space scattering cluster calculation establishes the connection between the short-range order, as reflected in cluster size or final-state electron damping, and the line-widths of sharp absorption features near the 2p edge. Results are shown for amorphous and crystalline Si, and silicon oxides in the form of quartz, obsidian, and thin films on single-crystal Si substrates.

1. Introduction

X-ray absorption fine structure (XAFS) spectroscopy is ideally suited to the exploration of the onset of crystalline ordering in amorphous materials since it is a local structural probe and it requires neither translational nor orientational order in the sample, unlike most diffraction probes. Extended x-ray absorption fine structure (EXAFS) measures oscillations in x-ray absorption cross-section beginning $\approx$ 50 eV above the absorption edge, which are used to measure the interatomic distances between the absorbing atom and its near neighbours. Usually EXAFS are recorded near deep core levels since core level energy separations must be large enough to allow measurements over an extended energy range. For example, Si 1s EXAFS has been used to determine the nearest neighbour Si–O and Si–Si bond distances in amorphous SiO_x compounds [1]. However, because of the relatively short core-hole lifetime of deep core levels, the information available in EXAFS experiments is limited to radial distances including only the first two or three nearest neighbours of an absorbing atom.

On the other hand, spectroscopy of the near-edge region in the range 0–50 eV from an absorption edge is usually regarded as a probe of electronic structure. Since the variation in the atomic cross-section is a smooth function of x-ray energy, the x-ray absorption near-edge structure (XANES) spectrum primarily reflects the local density-of-states (LDOS) of the unoccupied orbitals near the absorbing atom, modified to account for the dipole operator selection rules. The close connection between XANES and band-structure of a crystalline material is well known [2].

An equally valid theoretical description of the origin of XANES can be based on a local electron scattering theory in a finite cluster of atoms [3, 4]. Because of the finite electron

¶ Current address: IBM Research Division, Almaden Research Center, 650 Harry Road, San Jose, CA 95120-6099, USA.

0953-8984/93/315377+12$07.50

mean free path, the cluster model calculation is guaranteed to converge for a sufficiently large cluster, for which the results should be identical to that of a band-structure type calculation for an infinite crystal [2]. The description of XANES in terms of a real-space cluster model suggests that near-edge spectroscopy may also be used for structural studies, and in fact it may have some advantages over EXAFS. For example, XANES spectra may be collected for shallow core level excitations, for which the core-hole can have a longer lifetime than for deeper core levels. This implies that, in principle, XANES may be sensitive to crystal structure on length scales longer than those of EXAFS, and XANES might be useful in the study of order in semi-crystalline systems.

We have studied the XANES spectra above the Si 2p edge in ordered and disordered silicon and silicon oxide samples, both experimentally and (for the Si case) with a cluster multiple-scattering theory. The experimental measurements were done with sufficient energy resolution to identify changes in the XANES as the degree of crystalline order in the samples was changed. The line-widths of narrow XANES features, particularly in the oxide samples, were found to be particularly sensitive to disorder over length scales of several nanometers. Using the cluster multiple-scattering model, three sources of line-width broadening were found to be necessary to explain the experimental results. These included the intrinsic core-level lifetime, the final-state electron lifetime due to inelastic scattering, and a structural coherence length representing the degree of short-range order in the samples.

The calculations were performed using the cluster method developed by Durham, Pendry and Hodges [3] and Vvedensky, Saldin and Pendry (ICXANES) [4]: this is a full multiple-scattering technique, in which a nearly spherical cluster of atoms is divided into concentric shells containing atoms at nearly the same radius from the emitting atom at the centre. The XANES spectrum is found by evaluating the amplitude of the wavefunction that is reflected by the cluster back to the origin. A modification of the theory to calculate the transmitted amplitudes has been used to compute angle-resolved photoelectron and Auger electron diffraction patterns [5].

Experimental measurements were done using an x-ray photoemission electron microscope (XPEEM), which acts as a secondary-electron yield detector [6]. Use of the XPEEM for x-ray absorption measurements resulted in an improvement in energy resolution of about a factor of two over total electron yield techniques, because the imaging function of the XPEEM acted as a virtual monochromator exit slit of very small size. This enhanced energy resolution was useful in the studies of the narrow core-exciton lines of silicon-oxides.

The contribution of the core-hole lifetime to the line-width of sharp features in XANES can be very small. For example, recent high-resolution XANES of the 2p core-levels in transition-metal oxides show peaks as narrow as a few tenths of an eV [7]. The number and relative intensity of these peaks has been adequately described by an atomic model with crystal-field splitting [8]. The core-hole lifetime contribution to the Si 2p XANES is also small, but an atomic theoretical approach does not appear promising, since the electron final-states are more delocalized in Si than in the transition metal oxide systems.

The intrinsic core-hole lifetime is not the only important contribution to the line-width measured in the Si XANES spectrum, however. The finite range of the electron, which is caused by inelastic scattering, finite size of the atomic cluster, or random disorder, also contributes in a significant way. While the effects of core-hole lifetime broadening are independent of the final-state electron energy, the other contributions to broadening must vary with energy. Lifetime broadening can be incorporated into the theoretical model by adding a small constant imaginary part to the muffin-tin potential. We extend this model by incorporating energy dependent terms in the imaginary part of the innerpotential, to account for the electron mean free path and structural disorder.

2. Cluster multiple scattering method

The silicon L_{23} edge has been studied with increasingly sophisticated theoretical models since the late 1970s. The first work compared the absorption edge to the calculated total density of states (DOS) above the Fermi level [9], showing qualitative agreement between experiment and theory. Better agreement with experiment was found by calculation of the angular- momentum projected local DOS (p-LDOS) [10, 11], since although the DOS at the Fermi level has s, p and d character, only transitions to the s and d states are allowed in the $L_{2,3}$-edge spectrum. Further improvement was found by properly weighting the s and d channels with the appropriate energy-dependent photoemission matrix elements [12, 13].

This earlier work dealt with the structure within about 5 eV of the absorption edge, due to limitations in the band-structure method of computation at high kinetic energy. The band-structure methods all use some form of localized atomic orbitals in the basis set for the final states, which are not appropriate for calculations far above the Fermi edge. For high-energy calculations, a scattering formalism is more efficient, which is the approach taken in this work. The Si $L_{2,3}$ level absorption up to 40 eV above the edge is calculated by the multiple-scattering cluster method. In the language of the previous paragraphs, both the p-LDOS and the energy-dependent photoemission matrix elements are included.

The calculations were done using the IC-XANES programs [3, 4], substantially modified to allow non-s-state initial states. An ideal silicon crystal was modelled by an atomic cluster, with atoms divided into a series of shells of increasing radius (see table 1). The largest cluster included 46 silicon atoms surrounding the electron emitter, arranged into four shells, including all atoms within 8 Å of the emitter. Full intra-shell and inter-shell multiple scattering was included.

Table 1. Dimensions of atomic clusters.

Shell number	Number of atoms	Radius
1	4	2.35 Å
2	12	3.84 Å
3	12	4.50 Å
4a	6	5.43 Å
4b	12	5.92 Å

Scattering of the final-state electron was described by spherical waves in an exact Green's function representation. Atomic scattering phase shifts for angular momenta up to $l_{max} = 3$ were used for the scattering centred on each atomic nucleus. The shell scattering matrices are constructed by projecting the scattered waves at the atom sites in the shells onto an angular momentum basis set centred on the origin. This single-centre approximation step is computed with angular momentum terms up to l_{sc}, which is made energy dependent, to maximize calculation efficiency. A value of $l_{sc} = 1.5kr_{max}$ was used, up to a maximum of $l_{sc} = 31$, where r_{max} is the radius of the outermost atomic shell.

The atomic phase shifts and the silicon matrix elements were calculated with a muffin-tin potential model, using the Mattheis prescription [14]. The value of the muffin-tin zero (V_0) was treated as a fitting parameter, and best agreement with experiment was found with $V_0 = -13.3$ eV. Slater's Xα approximation was used for the exchange–correlation potential, with $\alpha = 0.7275$. The potential for the absorbing atom was chosen for neutral Si, as it was found that using an ionized or partially ionized atom, or using an aluminum atom emitter ($Z + 1$ approximation) had no significant effect on the results. The $L_{2,3}$ spin–orbit

splitting was incorporated using an energy separation of 0.61 eV and intensity ratio of 0.7, determined empirically [15].

Both the core-hole lifetime and final-state electron lifetime contribute to electron damping, which broadens the features in the XANES spectrum. The finite energy bandwidth of the core-hole (ΔE_c) is incorporated in the calculation by adding a constant imaginary component to the inner potential V_0, so that $V_0 = V_r + iV_i$, where $V_i = \frac{1}{2}\Delta E_c$. The electron damping then takes the form of an exponential damping factor e^{-qr}, where q is the imaginary component of the electron wavevector, given by

$$q = \frac{1}{a_0}\sqrt{\frac{1}{\epsilon_0}\left(\sqrt{\epsilon^2 + V_i^2} - \epsilon\right)} \tag{1}$$

which results from Schrödinger's equation for complex energy and wavevector. Here, $\epsilon = E - E_f$ is the electron kinetic energy, ϵ_0 is one Hartree, and a_0 is one Bohr radius.

For deep inner-shell core-levels, in which the core-hole lifetime leads to an energy broadening of the order of 1 eV, this broadening dominates over the electron lifetime effects, which can be therefore ignored in the near-edge region. For soft x-ray spectra, however, the core-hole lifetime broadening is very small (of the order of a few tenths of an eV). Good agreement between theory and experiment could not be obtained for the silicon L-edge without correcting for the additional damping due to the finite electron mean free path. Therefore, as is done for EXAFS calculations [16], we have introduced an energy dependent component of the imaginary potential, V_{inel}, to account for the effects of inelastic electron scattering [17]. This potential is related to the inelastic mean free path damping factor $q_{\text{inel}} = 1/2\lambda_{\text{MFP}}$, which is calculated from the empirical formula of Seah and Dench [18]:

$$1/q_{\text{inel}} = 2d\left[\frac{538}{\epsilon^2} + 0.13(d\epsilon)^{1/2}\right] \tag{2}$$

where d is the atomic diameter in angstroms, and ϵ is the energy in eV.

The total damping due to core-hole and final-state effects is then calculated from equation (1) using a potential that is the sum ($V_{\text{im}} = V_c + V_e$) of the core-hole broadening ($V_c = 0.2$ eV) and the electron damping found from [17]:

$$V_e = q_{\text{inel}} a_0 \sqrt{2\epsilon\epsilon_0}. \tag{3}$$

The resulting effective electron mean free path is shown in figure 1.

The effective electron mean free path shows a maximum about 5 eV above threshold of about 15 Å, where it is dominated by the small core-hole lifetime. In contrast, a deep core-hole lifetime of 1 eV would produce a maximum of only 6 Å. The longer electron mean free path for the shallow 2p core-hole means that a larger cluster size is necessary to correctly model the sharp structure near threshold. Also, since the mean free path near threshold is largely determined by the narrow core-hole linewidth, the measured or calculated linewidth can in turn be related to structural disorder over length scales set by the mean free path.

3. Experimental methods

The XANES measurements were made in an x-ray secondary electron photoemission microscope [6, 19, 20] at the Synchrotron Radiation Center (Wisconsin, USA) using monochromatic x-rays from 3M and 6M toroidal grating monochromators. The detected signal is composed of low energy electrons (secondaries) with a transmission function proportional to $1/E$ [6]. The secondary electron yield intensity $I(\hbar\omega)$ is related to

the photoabsorption coefficient by the relation $I(\hbar\omega) = \hbar\omega \times \mu(\hbar\omega)$ [21]. The microscope permits simultaneous observation of surface morphology during spectroscopic measurements. Typically, an area of 10 micron diameter is isolated in the microscope image and the signal from this region is integrated for the XANES spectrum.

The silicon samples were 1 cm^2 pieces cleaved from device quality (100) oriented wafers (Monsanto). Under ultra-high vacuum, the samples were annealed to 500 °C to remove adsorbed water and organic contamination, but to retain the 15 Å thick native oxide for XANES measurements [15, 22, 23]. A clean crystalline Si surface is prepared by further annealing the sample to about 1000 °C. The base pressure in the microscope column was 2×10^{-10} Torr. During heating of the silicon wafers the pressure was maintained below 1×10^{-9} Torr except during the short period when the native SiO_2 layer desorbs, at which time the pressure rose briefly to 1×10^{-8} Torr.

Sample surface composition of the single-crystal silicon samples was checked in additional experiments using identical preparation techniques, and analysis by x-ray photoelectron spectroscopy, Auger electron spectroscopy, and low-energy electron diffraction. These measurments verified the thickness of the native oxide, and showed that no measureable amount of carbon (or other surface species) was present after the 500 °C annealing treatment for the majority of samples. Occasional samples showed as much as 1/4 monolayer of carbon contamination, which may have been due to variations in sample mounting methods. The XANES measurements were therefore repeated on a large number of samples to ensure reproducibility.

Bulk silicon oxide samples were prepared by crushing small amounts of material into a powder and pressing the powders into indium foil, to reduce the effects of sample charging.

4. Comparison of theory and experiment: clean Si

The results of the XANES multiple-scattering calculation for the L-edge is compared to experiment in figure 2. The calculation shows good agreement over the entire energy range from the absorption edge to 50 eV above the edge. Above the absorption edge, there are two narrow resonances seen in both experiment and theory, and a broad resonance between 115 and 135 eV.

The sharp edge structure at 100 eV in the theory is a direct result of the calculation and is not the result of a Fermi-level cut-off. In the vicinity of the Fermi level, the calculation reproduces the low density of states in the Si bandgap, and the edge (see figure 2) is due to the states at the conduction band minimum. The calculation correctly reproduces the number and energy position of the structures near the absorption edge. There is also good agreement between theory and experiment on the energy broadening of structures at higher photon energy, caused by the energy-dependent imaginary part of the inner potential (see figure 1). As discussed above, the increase in V_{im} with increasing electron energy makes the low energy resonances sharper than those at higher energy.

Previous comparisons of theory and experiment have successfully related many of these XANES structures to critical points in the calculated conduction bands. Moving from low energy to high, three such structures are (i) the sharp onset of the absorption edge at the Δ_1 point, (ii) the first maximum near 101 eV from a DOS maximum in the L_1 band, and (iii) a smaller maximum at around 103 eV, from a DOS maximum in the L_3 band [11, 24].

The cluster XANES calculation is readily decomposed into the individual angular momentum channels, and this has been done in figure 3. We find that the sharp threshold at the Si $L_{2,3}$ edge is largely due to transitions to s states, in agreement with earlier calculations using band theory by Weng *et al* [13]. However, in contrast to an earlier

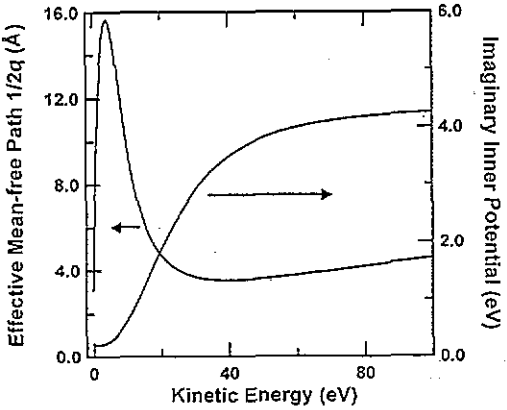

Figure 1. Calculated electron damping factor and imaginary potential including core-hole lifetime and final state lifetime effects.

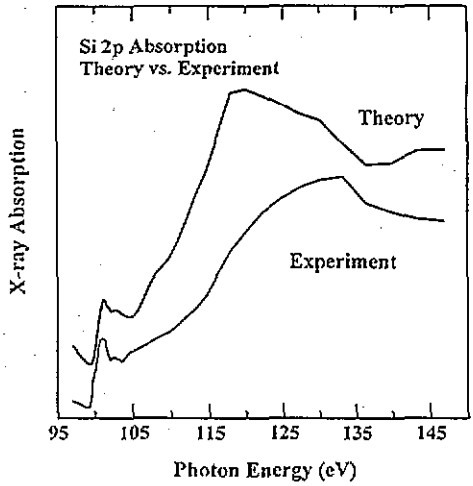

Figure 2. Comparison of calculated XANES spectrum with experiment, for single-crystal silicon. The theoretical data was convolved with two delta functions separated by 0.61 eV to simulate the spin–orbit splitting of the experiment.

study by Bianconi *et al* [10], we find that there are also substantial d-state contributions near threshold, which are responsible for the two sharp resonances at 101 eV and 103 eV. The energy dependence of the s and d state contributions near threshold is in agreement with band-structure calculations [13], and can also be understood in terms of the occupancy of silicon hybridized orbitals. For the ground-state $3s^1 3p^3 3d^0$ configuration of silicon, we expect unoccupied s and p states just above the Fermi level, with d states at higher energy. Of course the total spectrum (s plus d) is the result of the interference between these two channels, not simply the sum.

The broad resonance extending from about 115 to 135 eV in both theory and experiment is a result of the delayed onset effect [29] in the atomic absorption cross-section due to the centrifugal barrier in the atomic potential (see discussion of figure 4 below).

The present multiple-scattering calculation agrees as well with experiment as any prior work [9, 10, 12, 13]. This shows that the muffin-tin potential scattering approach to the calculation of near-edge structure (and equivalently of the unoccupied DOS) can be used for semiconductors with directional bonds. At least for the case of silicon, self-consistent potentials were not required for good agreement to experiment, in contrast to the expectations for other systems with highly directional bonds, such as chemisorbed atoms on surfaces [27]. The fact that core-hole corrections to the potential (such as the $Z + 1$ approximation [28]) were not required shows that final-state screening effects are not significant in the Si L-edge spectrum.

There are some variances between theory and experiment, however. One important difference is that the theoretical linewidths of structures near threshold are broader than those of the experiment. This effect is caused by the finite size of the atomic cluster used in the calculation. As shown in figure 1, the atom cluster radius should be $\geqslant$ 15 Å to reproduce structure at $\leqslant$ 5 eV above the edge. However, a cluster radius of only 8 Å was practical at this time, since the computational time scales as approximately the sixth power of the radius. A truncated atomic cluster produces an additional broadening, which can be estimated by using the relationship between inner potential and electron damping shown

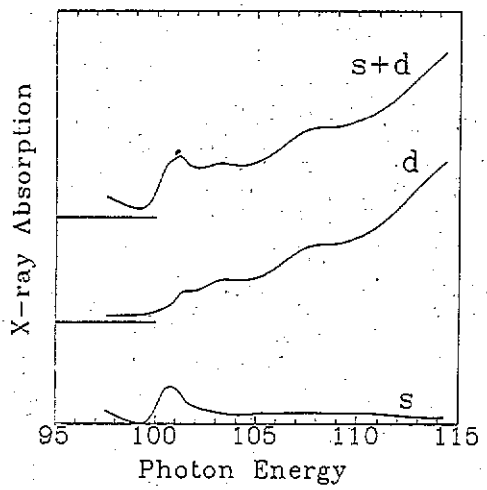

Figure 3. Decomposition of silicon 2p XANES calculation into s-wave and d-wave emission channels. It is seen that the edge structure and the first intensity maximum have s character, while the second maximum and the broad higher energy structures are primarily d-like in character.

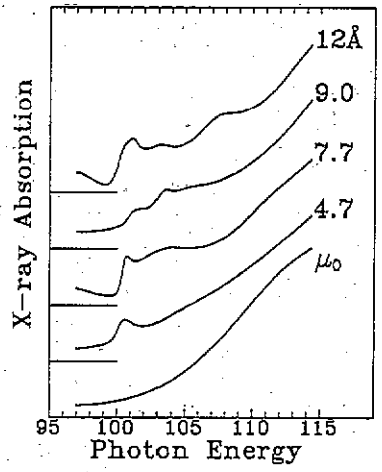

Figure 4. XANES calculations for small clusters of silicon atoms. The labels refer to the cluster diameter. The atomic absorption coefficient (bare atom) is shown at the bottom.

in equation (3). At 5 eV electron kinetic energy, a cluster radius of 8 Å corresponds to an effective imaginary inner-potential value of 1 eV. This is in agreement with the energy broadening observed in the calculation as compared with experiment at the absorption edge, which is found to be 1.0 eV. The core-hole and final-state lifetime broadening contribution is only 0.3 eV at this energy, so the additional broadening is due to the finite cluster size.

5. Finite cluster-size effects

The relatively long electron mean free path at the silicon $L_{2,3}$-edge makes the XANES spectra sensitive to the degree of short-range-order in the sample. We have attempted to model the effects of disorder in two ways. The first is to theoretically study small silicon molecules, which serve as a model in which perfect short range order is maintained, but the particle is embedded in a glassy host. This exercise allows us to use the real-space structure of the cluster XANES calculation to associate particular spectral features with specific atoms in the cluster. The second technique used was to increase the size of the imaginary inner potential, using equation (1), to model an effective coherence length (ξ) over which short-range order is preserved.

Silicon molecules with bulk silicon bond lengths were constructed in the shell model, consisting of from one to four shells. Atom locations and numbers are shown in table 1. The results of the calculations for all four clusters are shown in comparison to the silicon atomic absorption coefficient in figure 4. There are relatively large changes in the spectral shape with cluster size apparent in this figure. Given the changes seen between the 3- and 4-shell cluster (with diameter 9.0 Å and 12.0 Å respectively), it could not be determined from this series alone that the results have converged in terms of cluster size, and it is possible that a larger cluster would show some change from that of the largest cluster attempted in this work. The principle reason for confidence in the calculation at this stage is the relatively good agreement between theory and experiment.

6. Electron damping model of disorder

Experimentally, disorder was introduced into the silicon surface region by sputtering with 5 keV argon ions for several minutes. This produces an amorphous silicon layer which produces no LEED pattern. We show a comparison between theory and experiment for the ordered and amorphous surfaces in figure 5. The experimental data has had the spin–orbit splitting removed by deconvolution [15, 23].

The effects of disorder on K-shell EXAFS were incorporated into a path-formalism series expansion theory by modifying the Debye–Waller factor to include both a thermal disorder and a configurational disorder term [25, 26]. This approach is not effective in our exact matrix inversion cluster formalism, since the Debye–Waller thermal disorder effects are included by modifying the scattering phase shifts. This would require a new set of phase shifts to be computed for each modelled degree of disorder.

Instead, we model structural disorder with the introduction of an additional electron damping factor through a new term in the imaginary inner potential. The magnitude of the contribution to the inner potential due to structural disorder, V_ξ, can be related to an electron coherence length ($\xi = 1/q$) through an expression similar to equation (3). The physical justification for this approach is that it approximates a situation in which the sample has good short range order (over distances comparable to ξ), but that for distances much longer than ξ the atoms in a shell can be considered to be randomly distributed and therefore do not contribute to the near-edge peaks.

The overall effect of both the structural Debye–Waller term [26] and our structural coherence length is an exponential damping of the electron wave with distance from the emitting atom ($e^{-r/\xi}$), which limits the size of the cluster that contributes to the XANES intensity. The advantage of the structural Debye–Waller factor approach is that it can be used to directly relate the displacement of atoms from their mean positions to the structural coherence radius, whereas in our method this coherence length is purely empirical. For example, a value of the electron coherence length of $\xi = 13$ Å was used in the calculation shown in figure 5, which gives reasonable agreement with the experiment.

The main difference between the experimental data for ordered and disordered silicon surfaces is the absence of sharp spectral features above the absorption edge in the sputtered surface. This effect is accurately reproduced with the additional damping factor to model a finite electron coherence length. We conclude that the line-width of structures in the Si L-edge XANES is the result of contributions from the core-hole lifetime, final-state lifetime (inelastic scattering), and structural disorder.

7. Linewidths in silicon dioxide XANES

Although we have not yet attempted to apply the full multiple-scattering formalism developed for pure Si to the case of silicon oxides, we present here some experimental results from oxides that suggest that such a calculation is worth pursuing.

There are at least eight crystalline forms of SiO_2 in nature. Usually, the low-temperature phases are the most complex. The simplest form of crystalline SiO_2 is high-temperature cristobalite, which has a diamond lattice that can be visualized by taking elemental silicon and inserting an oxygen atom into every silicon–silicon bond. All other forms of crystalline silicon dioxide are simply variations of this structure with reduced symmetry.

Because of multiple-scattering effects, it has been argued [30] that such subtle structural disturbances could generate detectable changes in the XANES spectra, whereas they would

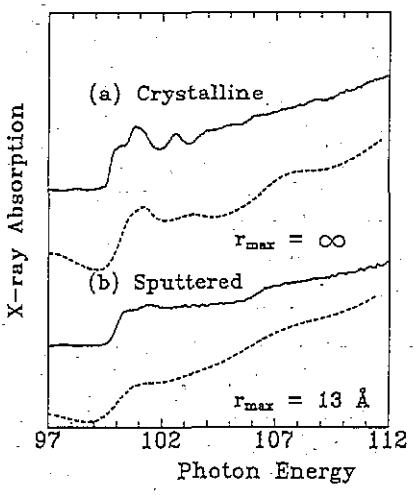

Figure 5. Experimental XANES (solid lines) from crystalline and amorphous silicon compared with XANES calculations (dashed lines) assuming differing crystalline coherence lengths, ξ, as labeled. The amorphous silicon was prepared by sputtering a single crystal sample for several minutes at room temperature. In the calculation with $\xi = 13$ Å, the coherence length was chosen to give the best agreement with experiment.

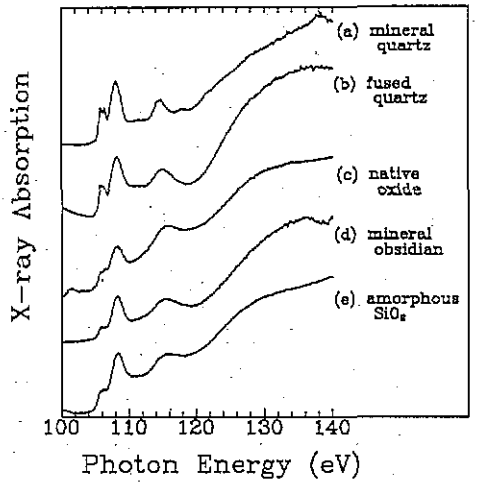

Figure 6. XANES spectra from several forms of SiO_2, including mineral quartz, fused or glassy quartz, 15 Å native oxide on Si(100), mineral obsidian, and 50 Å of amorphous SiO_2 on single crystal silicon. Note that all the spectra look quite similar. The samples with increased disorder, such as amorphous SiO_2 on single-crystal silicon, show the same XANES structures, with some spectral broadening.

not be visible in the single-scattering region of the spectrum characterized by the EXAFS oscillations.

We have measured the Si $L_{2,3}$-edge XANES from several forms of SiO_2, as shown in figure 6. The five samples studied include mineral quartz, fused or glassy quartz, a native-oxide film on Si(100), obsidian (a natural glass), and a 50 Å thick amorphous oxide film. Note that all spectra show very similar structures. Each is characterized by a sharp core exciton feature at 105.8 eV, which appears as a spin–orbit doublet [15, 22]. Additional resonances are found at 108 eV, 115 eV, and 130 eV.

Differences between the spectra of the different materials are small. The most evident effect is a change in line-widths, particularly at the core-exciton, which can be accounted for by an energy dependent spectral broadening of the form discussed above for pure silicon. For these silicon oxides, we find that the XANES spectra are identical except for effects due to varying amounts of long-range order, and changes due to the small differences in crystal structure are not detected.

Three of the oxide spectra are shown on an expanded scale in figure 7. These include mineral quartz, fused quartz, and the native oxide, which are labeled 3D crystal, 3D amorphous, and 2D crystal respectively. The sample with the highest degree of long-range order (3D crystal, mineral quartz), shows a spin–orbit doublet at the core-exciton with a line-width close to the experimental resolution. In comparison, the spectrum from fused quartz (3D amorphous) is simply a broadened version of the mineral spectrum. It is well known [31] that the structure of fused quartz is not entirely amorphous, but retains short-range order with a coherence radius of 15–20 Å, which includes the first 5 or 6 atomic shells.

We propose that the line-width of the core-exciton in these silicon oxides is determined in part by the degree of short-range order in the sample. The line-width has contributions from

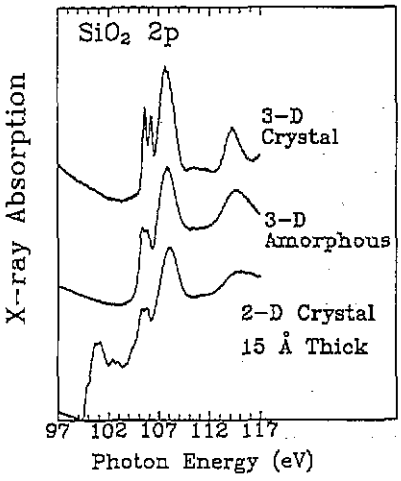

Figure 7. The mineral quartz (3D crystal), fused quartz (3D amorphous), and native oxide (2D crystal), spectra from figure 6 shown on an expanded scale. Mineral quartz has nearly perfect three-dimensional crystalline order throughout, fused quartz is a three-dimensional system with a large amount of crystalline disorder, and the native oxide is a reduced dimensional system containing some disorder. Both disorder and crystal truncation cause spectral broadening in these XANES spectra.

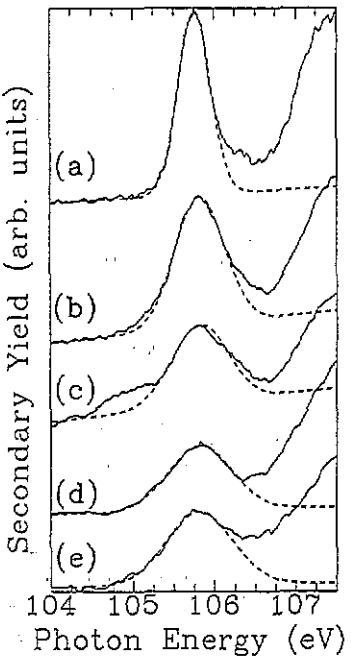

Figure 8. The core exciton structures of figure 7 plotted on an expanded scale (solid lines). These spectra are (a), mineral quartz, (b), fused quartz, (c), native oxide, (d), mineral obsidian, and (e), 50 Å of amorphous SiO_2 on Si(100). Superimposed upon these structures are Gaussian curves which showed the best fit with the data (dashed lines).

the core-hole and final-state electron lifetimes, as discussed above for silicon. The magnitude of these contributions can be determined from the data for crystalline quartz, which has a measured linewidth of 0.41 eV. The spectra for fused quartz, native oxide, obsidian, and amorphous quartz all show larger linewidths. This additional linewidth broadening is attributed to a combination of structural disorder and finite-size effects.

To model the additional broadening from disorder, we assume that there is a coherence length ξ, which characterizes the mean radius of clusters of atoms with perfect short-range order. This coherence length must be modified, in the case of an epitaxial film, to account for the finite film thickness. As discussed for the comparison of crystalline and amorphous Si, the coherence length can be converted into a line-width contribution using the relation $V_\xi = \sqrt{2\epsilon\epsilon_0}/(\xi/a_0)$ (equation (3)), which is the small V_ξ limit of equation (1). Because we expect the sample to be composed of an ensemble of clusters with varying degrees of short-range order, the contribution from disorder, V_ξ, is added in quadrature to the imaginary potential derived from core-hole and final-state lifetimes.

The oxide core-exciton lines, with spin–orbit contributions deconvolved, are shown on an expanded scale in figure 8. The spectra are plotted in the sequence mineral (crystalline) quartz, fused quartz, native oxide film, obsidian, and 50 Å thick amorphous oxide. In this order, the exciton line-width is progressively broader, indicating a decrease in the degree of short-range order. Note that in the native oxide spectrum there is an additional peak at

104.7 eV, which is due to an interfacial oxide state. This interface component has been discussed in detail elsewhere [15, 22, 23].

Table 2. Linewidths SiO_2 core-exciton line-widths and inferred coherence lengths.

Material	Measured FWHM	Less inst.	Coherence radius
Quartz crystal	0.46	0.41	∞
Fused quartz	0.72	0.69	17 Å
Obsidian	0.82	0.80	13 Å
Native oxide	0.82	0.80	13 Å
Amorphous oxide	0.97	0.95	10 Å

The exciton line-widths are given in table 2, which used an instrumental resolution of 0.2 eV. The additional broadening due to local disorder is expressed as a coherence radius, which is derived using an intrinsic linewidth taken from the quartz crystal data. The value of the final-state electron energy in the solid was found to be $\epsilon = 4.6$ eV, which yields the correct value of 17 Å for the coherence radius in fused quartz [31].

The degree of local disorder in the amorphous oxide film is found to be substantially larger than that of bulk fused quartz, as reflected in the reduction of the coherence radius from 17 Å to 10 Å. We also find that the coherence radius for the native oxide, at 13 Å, is larger than that of the amorphous oxide, and is comparable to the thickness of the film. The two-dimensional geometry of the native-oxide is itself a source of line-width broadening. Thus, the derived coherence radius of 13 Å is a lower bound on the short-range order in the film, since the model assumed a three dimensional infinite solid. Incorporating the effects of the restricted geometry in a simple way [23] gives a value of over 20 Å for the coherence radius parallel to the surface of the native oxide film. This suggests that the native oxide has a degree of local order comparable to fused quartz, and measureably higher order than the amorphous oxide. The native-oxide samples studied here were prepared by annealing to 500 °C, which was found to reduce the linewidth by a small amount [15, 23], and which we interpret as resulting in an improvement to the short-range order.

8. Conclusion

We find that the cluster multiple scattering method using neutral silicon atom muffin-tin potentials, when extended to calculate the XANES for an $l = 1$ orbital, gives good agreement to experiment for the case of Si 2p levels both at the edge and up to 50 eV above the edge. An accurate explanation of the measured line-widths in the crystalline semiconductor requires a complex potential that includes contributions from both the core-hole lifetime and electron final-state lifetime, with a value of the imaginary part of the inner potential that reaches a saturation value of 4 eV by 60 eV above the edge, but falls to the core-hole lifetime value of 0.2 eV near threshold.

High resolution XANES spectra from a series of oxides show a similar core-exciton feature in all cases, which can be identified by a characteristic spin–orbit splitting. After removal of instrumental effects and spin–orbit deconvolution, the line-widths of the core-exciton are found to vary with the degree of short-range order in the samples. A model that incorporates a coherence radius can be used to correlate the short-range order in a sample with measured XANES line-widths.

Structural disorder in both elemental silicon and silicon oxides is found to produce a broadening of absorption resonances near threshold, which is observable because of

the small contribution of core-hole and final-state lifetime broadening at low energy. A semi-empirical model based on a structural coherence length was incorporated into the full multiple-scattering calculation and was found to qualitatively reproduce measured effects. Future theoretical work should include a comparison to calculations using an alternative formulation of structural disorder based on Debye–Waller effects [25].

Acknowledgments

We are grateful to Z L Han and Lee-Jene Lai for assistance with some of these experiments. The measurements were performed at the Synchrotron Radiation Center, which is supported by the National Science Foundation. The work was supported in part by the Petroleum Research Foundation (DKS) and by grant DMR-91-15987 from the National Science Foundation (BPT).

References

[1] Greaves G N 1985 *J. Non-Cryst. Solids* **71** 203
[2] Schaich W L 1973 *Phys. Rev.* B **8** 4028
[3] Durham P J, Pendry J B and Hodges C H 1982 *Comput. Phys. Commun.* **29** 193
[4] Vvedensky D D, Saldin D K and Pendry J B 1986 *Comput. Phys. Commun.* **40** 421
[5] Saldin D K, Harp G R and Tonner B P 1992 *Phys. Rev.* B **45** 9629
[6] Tonner B P and Harp G R, Koranda S F and Zhang J 1992 *Rev. Sci. Instrum.* **63** 564
[7] van Elp J, Eskes H, Kuiper P and Sawatzky G A 1992 *Phys. Rev.* B **45** 1612
[8] van der Laan G and Kirkman I W 1992 *J. Phys.: Condens. Matter* **4** 4189
[9] Gahwiller C and Brown F C 1979 *Phys. Rev.* B **2** 1918
[10] Bianconi A, Del Sole R, Selloni A, Chiaradia P, Fanfoni M and Davoli I 1987 *Solid State Commun.* **64** 1313
[11] Batson P E 1991 *Phys. Rev.* B **44** 5556
[12] Ma H, Lin S H, Carpenter R W and Sankey O F 1990 *J. Appl. Phys.* **68** 288
[13] Weng X, Rez P and Batson P E 1990 *Solid State Commun.* **74** 1013
Weng X, Rez P and Sankey O F 1989 *Phys. Rev.* B **40** 5694
[14] Mattheiss L F 1964 *Phys. Rev.* A **133** 1399
[15] Harp G R, Han Z-L and Tonner B P 1990 *Phys. Scr.* **T 31** 23
[16] Dan Lu, Mustre de Leon J and Rehr J J 1989 *Physica* B **158** 413
[17] Bianconi A and Marcelli A 1979 *Synchrotron Radiation Research* ed R Z Bachrach (New York: Plenum) p 69
[18] Seah M P and Dench W A *Surf. Interface Anal.* **1** 2
[19] Tonner B P and Harp G R 1988 *Rev. Sci. Instrum.* **59** 853
[20] Tonner B P and Harp G R 1989 *J. Vac. Sci. Technol.* A **7** 1
[21] Gudat W and Kunz C 1972 *Phys. Rev. Lett.* **29** 169
[22] Harp G R, Han Z-L and Tonner B P 1990 *J. Vac. Sci. Technol.* A **8** 2566
[23] Harp G R 1992 *PhD Dissertation* Univeristy of Wisconsin–Milwaukee
[24] Brown F C and Rustgi O P 1981 *Phys. Rev. Lett.* **8** 497
[25] Evangelisti F, Proietti M G, Balzarotti A, Comin F, Incoccia L and Mobilio S *Solid State Commun.* **37** 413
[26] Bianconi A, Di A Cicco, Pavel N V, Benfatto M, Marcelli A, Natoli C R, Pianetta P and Woicik J 1987 *Phys. Rev.* B **36** 6426
[27] See, for example, the discussion in
Stöhr J 1988 *NEXAFS Spectroscopy* (New York: Springer) ch 2
[28] Brydson R, Bruley J and Thomas J M 1988 *Chem. Phys. Lett.* **149** 343
[29] Manson S T and Cooper J W 1968 *Phys. Rev.* **165** 126
[30] Durham P J, Pendry J B and Hodges C H 1981 *Solid State Commun.* **38** 159
[31] Warren B E and Biscoe J E 1938 *J. Am. Ceram. Soc.* **21** 259